https://doi.org/10.2352/issn.2169-2629.2020.28.34

Inverse-Scaled Lanczos Filtering for Image Sharpening

Hiroaki Kotera, Kotera Imaging Laboratory, Chiba, Japan.

Abstract

The edge response in retinal image is the first step for human vision recognizing the outside world. A variety of receptive field models for describing the impulse response have been proposed. Which satisfies the uncertain principle? occupied the interest from a point of minimizing the product (Δx)($\Delta\omega$) both in spatial and spectral. Among the typical edge response models, finally ***Gabor*** *function and 2nd. Gaussian Derivative* $\boldsymbol{GD_2}$ *remained as strong candidates. While famous D. Marr and R. Young support* $\boldsymbol{GD_2}$*, many vision researchers prefer* ***Gabor****. The retinal edge response model is used for image sharpening.*

Different from the conventional image sharpening filters, this paper proposes a novel image sharpening filter by modifying the Lanczos resampling filter. The Lanczos filter is used for image scaling to resize digital images. Usually it works to interpolate the discrete sampled points like as a kind of smoothing filter not as sharpening. The Lanczos kernel is given by the product of sampling Sinc function and the scaled Sinc function. The scaled Sinc function expanded by the scale "s" plays a role of window function. The author noticed that the inverse scaling of Lanczos window can be used not for smoothing but for sharpening filter.

This paper demonstrates how the proposed model works effectively in comparison with Gabor and $\boldsymbol{GD_2}$**.**

Edge Response Models in Retina

The edge response in receptive field of retina was firstly modeled for cat's eye by Hubel & Wiesel [1]. The neural signal from visual cortex was mathematically described by *DOG* function and later won the Nobel Prize.

The key mathematical models include the followings.

- *Gaussian=exp*$[-x^2/2]$
- *Hermite Function=He (Type H) *Gaussian*
- ***GD* (*Gaussian Derivative*)**
  $=H_n$ *(Hermite Polynomials Type He)•Gaussian*
- *DOG* (*Difference-Of-Gaussian*)
- *DOOG* (*Difference-Of-Offset-Gaussian*)
- *DODOG* (*Difference-Of-Offset-DOGs*)
- *SODOG*(*Sum-Of-Offset-DOGs*)
- ***Gabor*=(*Cosine/Sine*)•*Gaussian***

Of these, there were intensive debates [2][3][4] about which satisfies uncertain principle to minimize the product (Δx)•($\Delta\omega$) that demands compact localization both spatially (Δx) and spectrally ($\Delta\omega$). Finally, ***Gabor*** function [5] and 2nd. Gaussian Derivative $\boldsymbol{GD_2}$ remained as strong candidates. While famous D. Marr [6] and R. Young [7] support $\boldsymbol{GD_2}$, many vision researchers prefer ***Gabor***. Based on the above background, the retinal edge response is modeled for designing the image sharpening filters.

Edge Detection Filters and Compactness

2nd Order Gaussian Derivative Filter

The one-dimensional (1D) Gaussian function is given as

$$g(x,\sigma)=\frac{1}{\sqrt{2\pi}\sigma}exp\left(-x^2/2\sigma^2\right) \tag{1}$$

Its n-th. order derivative becomes again Gaussian as given by

$$\begin{aligned} \boldsymbol{GD}_n(x,\sigma) &= \partial^n \boldsymbol{g}(x,\sigma)/\partial x^n \\ &= (-1)^n \frac{1}{(\sqrt{2}\sigma)^n} H_n\left(\frac{x}{\sqrt{2}\sigma}\right)\boldsymbol{g}(x,\sigma) \end{aligned} \tag{2}$$

Where, $H_n(x)$ denotes Hermitian polynomials.

The 2 nd. order derivative for 1D Gaussian function is given by

$$\boldsymbol{GD}_2(x,\sigma)=\nabla^2\boldsymbol{g}(x,\sigma)=\frac{\left(x^2-\sigma^2\right)exp\left(-x^2/2\sigma^2\right)}{\sqrt{2\pi}\sigma^5} \tag{3}$$

By Fourier transform theorem of n th. Gaussan derivative

$$\mathcal{F}\left\{\partial^n \boldsymbol{g}(x,\sigma)/\partial x^n\right\}=(-i\omega)^n\,\mathcal{F}\left\{\boldsymbol{g}(x,\sigma)\right\} \tag{4}$$

Hence, the Fourier (notated $\mathcal{F}$) spectrum of 2D Gaussian derivative for $\boldsymbol{GD_2}$ is described as

$$\begin{aligned} \boldsymbol{GD}_2(\omega_x,\omega_y,\sigma) &= \mathcal{F}\left\{\boldsymbol{GD}_2(x,y,\sigma)\right\} \\ &= \frac{1}{\sqrt{2\pi}}\left(\omega_x^2+\omega_y^2\right)exp\left[-\frac{1}{2}\sigma^2\left(\omega_x^2+\omega_y^2\right)\right] \end{aligned} \tag{5}$$

Figure 1(a) shows n (=1~7) the 1D Gaussian derivatives and their Fourier transforms. It is clear how compact these are localized both in spatial and in spatial frequency.

Figure 1(b) shows the profile of 2 nd. order 2D Gaussian derivative $\boldsymbol{GD_2}(x, y, \sigma)$ whose vertical axis is inversed negative and its Fourier transform. As well, it has compactly localized profiles in spatial (Δx) and in spatial frequency ($\Delta\omega$).

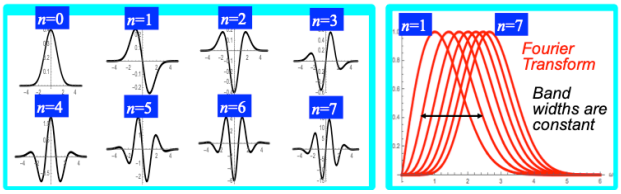

(a) One-dimensional n-th. Gaussian derivatives and Fourier spectra

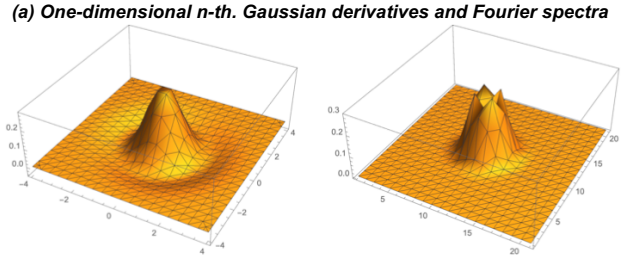

(b) Two-dimensional 2nd Gaussian derivative and Fourier spectrum

Figure 1 . Profile of Gaussian derivatives and Fourier transforms

Gabor Filter

The Gabor function is basically defined by the product of Sinusoidal function and Gaussian function. There are sine-type, cosine-type, and complex-type consisting of mixture of sine and cosine. Here, in practice, the real cosine-type is used.

The Gabor function is used for detecting the directional edges in images and/or visual spatial-temporal response analysis.

The 1D Gabor function is given by

$$\begin{aligned} \boldsymbol{g}_{abor}(x,\sigma) &= \boldsymbol{g}(x,\sigma)cos(\omega_0 x) \\ &= \frac{1}{\sqrt{2\pi}\sigma}exp(-x^2/2\sigma^2)cos(\omega_0 x) \end{aligned} \tag{6}$$

Daugman [8] extended 1D *Gabor* function to 2D. In the isotropic case of $\omega_x = \omega_y = \omega_0$, it's described as

$$g_{abor}(x,y,\sigma) = \frac{1}{2\pi\sigma^2} exp\left[-\frac{(x^2+y^2)}{2\sigma^2}\right] cos(\omega_0 x + \omega_0 y) \quad (7)$$

Applying Fourier transform to eq. (7), the spatial frequency spectral distribution is obtained as follows.

$$G_{abor}(\omega_x, \omega_y, \sigma) = \mathcal{F}\{g_{abor}(x,y,\sigma)\}$$
$$= \mathcal{F}\left\{\frac{1}{2\pi\sigma^2} exp\left[-\frac{(x^2+y^2)}{2\sigma^2}\right]\right\} * \mathcal{F}\{cos(\omega_0 x + \omega_0 y)\} \quad (8)$$

where, the symbol "*" denotes convolution integral.

Thus, eq. (8) means that the Fourier spectrum of 2D Gabor function equals that of 2D Gaussian function just shifted by $\pm\omega_0$ in the spatial frequency domain.

Figure 2 shows the shape of 2D Gabor function and its Fourier transform. As well as 2 nd. Gaussian derivative, 2D Gabor function is also compactly localized both in spatial and in spatial frequency. It may be used for image sharpening filter.

Figure 3 compares the cross-sectional profiles between a 2D Gabor function and a 2 nd. order Gaussian derivative. Both are shown to have very similar shapes. Though, the Gabor is necessary to set at least two parameters of (σ, ω). Care must be taken when applying these parameters, because the profile becomes complicated depending on the combination.

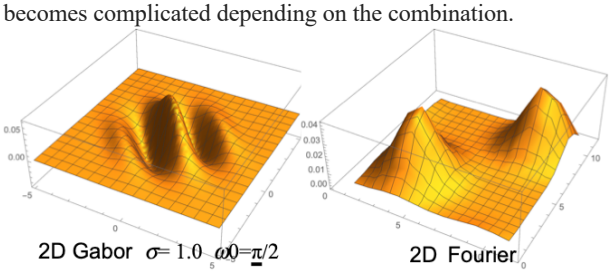

Figure 2 . Profile of 2D Gabor function and its Fourier transform

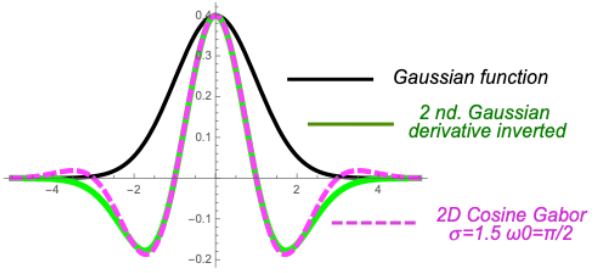

Figure 3 . Comparison in cross-sectional profiles between Gaussian derivative and Gabor functions

Inverse-Scaled Lanczos Filter

Different from the above-mentioned vision-based models, the following Lanczos Resampling function ***LR*** [9] is known. It performs smooth scaling by interpolating a sampled image.

LR is defined by the product of sampling *Sinc* function and the scaled *Sinc* function. 2D ***LR*** function is given as follows.

$$\boldsymbol{LR}(x,y,s) = Sinc(x)Sinc(x/s)Sinc(y)Sinc(y/s) \quad (9)$$

The scaled *Sinc* function expanded by the scale s plays a role of window function. As well known, *Sinc* function represents the ideal interpolation function for bandwidth limited signals when sampled and reproduced at Nyquist rate. ***LR*** combines the *Sinc* function with the window function *Sinc* (*x*/*s*) expanded by scale *s* (integer) to achieve smooth interpolation by blocking ringing.

However, since ***LR*** is a kind of smoothing filter, it cannot be used for sharpening as it is. Therefore, paying attention to the fact that the center of the *Sinc* function has a profile similar to the 2 nd. Gaussian derivative $\boldsymbol{GD}_2$, the author compressed the window function by the inverse of scale *s*. Thus, the inverse -scaled 2D *Lanczos* sharpening filter $\boldsymbol{LR}_{Sharp}$ is constructed as

$$\boldsymbol{LR}_{Sharp}(x,y,s) = Sinc(x)Sinc(sx)Sinc(y)Sinc(sy) \quad (10)$$

Figure 4 illustrates how the basic ***LR*** function changes into a sharpening filter by just replacing the scale with its inverse s^{-1}.

For example, a 2D $\boldsymbol{LR}_{Sharp}$ for s=5 has a very sharp profile like a needle. Its Fourier DCT shows unique block-shaped spectral distribution whose pass characteristics is flat inside the band and has a sharp cut-off outside the band. It can be said that $\boldsymbol{LR}_{Sharp}$ filter is also compactly localized both in spatial and in spatial frequency.

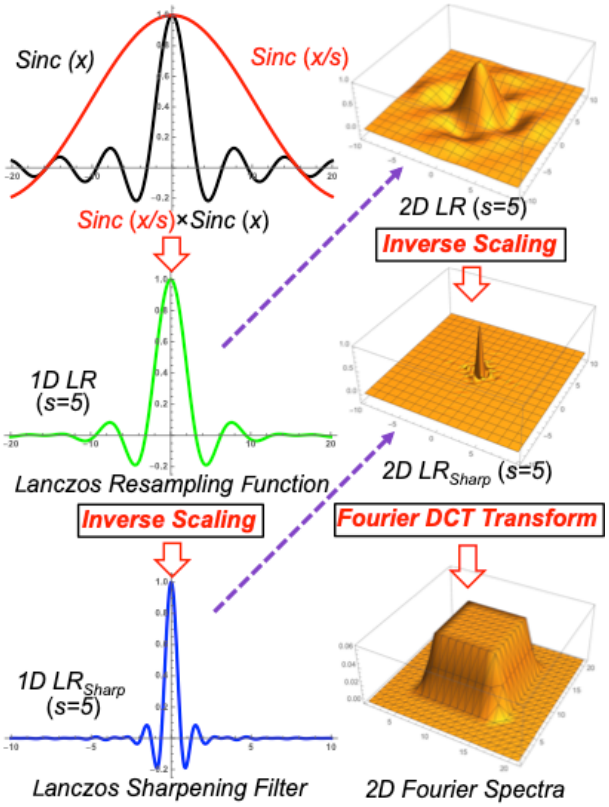

Figure 4 . LR into inverse-scaled LR_{Sharp} and its Fourier transform

Practical Application to Image Sharpening

Kernel Design of Image Sharpening Filter

In practice, the *Image Sharpening Filter* (***ISF***) is designed in discrete digital form considering the following conditions.

[1] The *Edge Detection Filter* (***EDF***) is approximated by $M \times M$ square matrix.

[2] The weights of filter should be equivalent to the local integral of continuous sharpening function in between discrete lattice points.

[3] The sum of ***EDF*** weights is initially set to zero not to respond to flat areas without edges. After that, adding 1.0 to the central element, the total sum of weights is finally adjusted to 1.0 to provide the ***ISF*** [10].

Figure 5 illustrates an example of kernel design for ***ISF*** using $\boldsymbol{GD}_2$ as the ***EDF***. The matrix size M of $\boldsymbol{GD}_2$ depends on the standard deviation σ. The cross sectional profile of $\boldsymbol{GD}_2$ in radial direction has the well-known Mexican hat shape with the zero cross points at radial distance $r_0 = \pm\sqrt{2}\sigma$ and the

minimum peaks at $r_1 = \pm 2\sigma$. The 2D $\boldsymbol{GD_2}$ function is approximated by $M \times M$ square matrix $\boldsymbol{W}=[w_{ij}]$ on discrete lattice points $[i, j]$.

To satisfy the condition [2], we take an odd integer $M=2m+1$ (m=1, 2, ...) and the weights $[w_{ij}]$ are calculated by the following local integral between the lattice points $[i, j]$.

$$w_{ij} = \int_{j-0.5}^{j+0.5}\int_{i-0.5}^{i+0.5} [-\nabla^2 G(x,y)]dxdy \qquad (11)$$

For example, in the case of m=3, the weights $\boldsymbol{W}=[w_{ij}]$ in 7× 7 matrix are designed as shown in the profile of *Figure 5*.

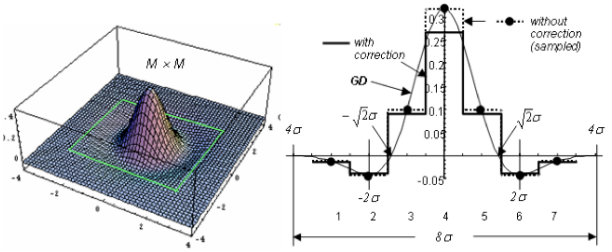

Figure 5 .Example of Image Sharpening Filter kernel design with GD_2

Image Sharpening Process

Image sharpening is obtained by convoluving the $\boldsymbol{ISF}(x, y)$ with an image $\boldsymbol{I}(x, y)$ as

$$\boldsymbol{I_{sharp}}(x,y) = \boldsymbol{ISF}(x,y) * \boldsymbol{I}(x,y)$$
$$* \text{ denotes convolution integral} \qquad (12)$$

where, $\boldsymbol{Gabor}$, $\boldsymbol{GD_2}$ or $\boldsymbol{LR_{Sharp}}$ is used for $\boldsymbol{EDF}$ to create the kernel of $\boldsymbol{ISF}$.

Figure 6 shows a comparison in the sharpened images by the proposed $\boldsymbol{LR_{Sharp}}$ and the typical conventional $\boldsymbol{EDF}$s.

Figure 6 . Comparison in sharpened typical image samples

At first glance, the simplest 3 x 3 Laplacian filtering appears to have the highest sharpness, but the contour is little bit over-emphasized and granular noise is also noticeable. On the other hand, $\boldsymbol{Gabor}$ seems to be under-emphasized. The proposed $\boldsymbol{LR_{Sharp}}$ shows better sharpness than $\boldsymbol{Gabor}$ and gives a good impression close to $\boldsymbol{GD_2}$. In the previous paper [10], we developed a sharpening method that adapts to the edge gradient and suppresses background noises in flat areas, but had the disadvantage of high computational costs. Since the proposed method does not incorporate this background noise suppression function, it is left behind as a future improvement.

Figure 7 (a) shows a comparison in the sharpened results for a standard test image "*Thread*" in *IIEEJ* SCID database and their Fourier DCT spectral distributions. As well, the 3 x 3 Laplacian filtering works well to enhance the details of yarn ball. Though, the edges are overemphasized and the colors look fading. This is a fatal drawback in color reproducibility. Also, $\boldsymbol{Gabor}$ lacks some sharpness. While, $\boldsymbol{GD_2}$ and $\boldsymbol{LR_{Sharp}}$ emphasize the texture of delicate yarn balls almost well. These sharpening effects are also accurately reflected in the Fourier DCT spectral distribution in *Figure 7* (b).

(a) Comparisons in sharpened "Tread" standard test image

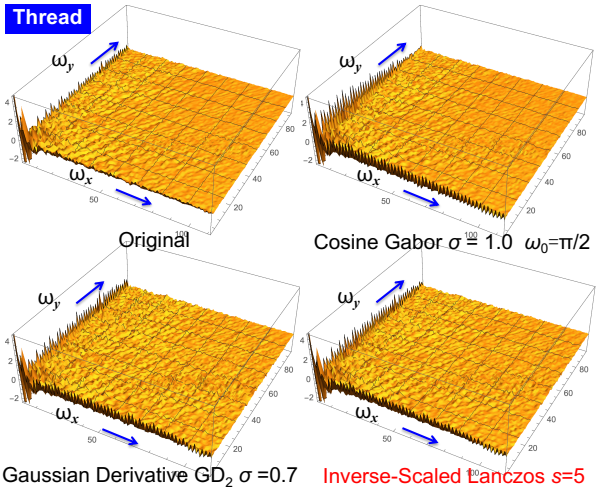

(b) Comparison in Fourier DCT spectral distributions

Figure 7 . Sharpened image "Thread" and Fourier DCT spectra

Figure 8 shows an example of "*Taj Mahal*", a total marble tomb in India, comparing the effects of reproducing the delicate structural patterns on the walls. (a) and (b) are the whole picture and the partial close up. In this example, the proposed $\boldsymbol{LR_{Sharp}}$ resulted in the best performance. It emphasizes the details of the delicate wall pattern most clearly.

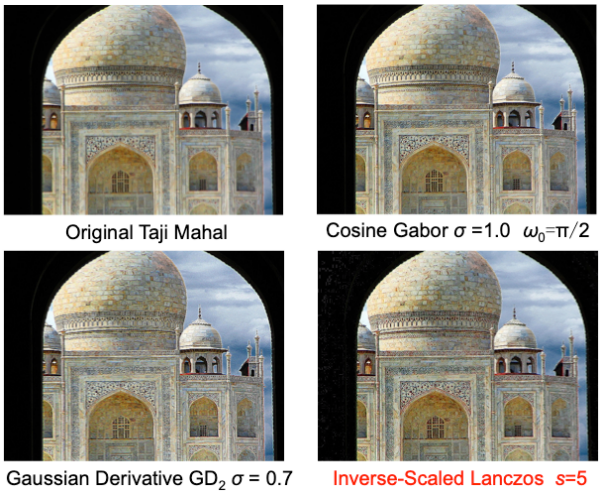

(a) Comparisons in sharpened "Taj Mahal" mausoleum

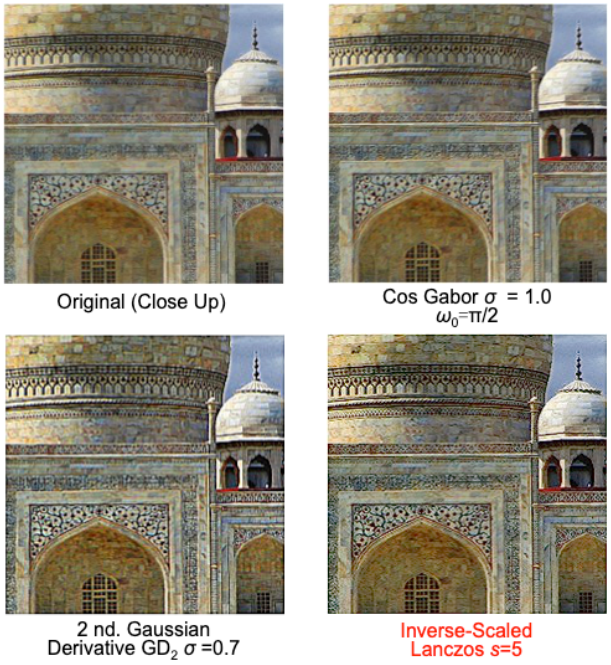

(b) Close Up of sharpened wall patterens in "Taj Mahal"

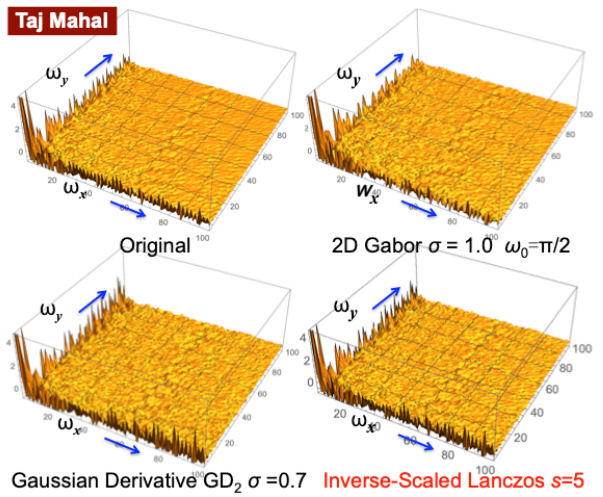

(c) Comparison in Fourier DCT spectral distributions

Figure 8. Sharpened image "Taj Mahal" and Fourier DCT spectra

Evaluation of Image Sharpness

Image sharpness is a very important factor in image quality assessment. Various methods for evaluating image sharpness have been developed. There are the following key concepts.

A) Spatial-based B) Frequency-based C) Hybrid of A) + B)

A statistical measure for SEM image sharpness is proposed by N. F. Zhang et al. [11], where the Kurtosis of multi-variate probability density function is defined by up to 4 the order moments and used for the image sharpness index. But advanced mathematical model is used and hard to use in practice.

A typical way is to measure edge strength such as edge width and edge gradient based on edge detection. Instead, edge blurriness such as JNB (Just Noticeable Blur) may be measured.

However, these edge-based techniques are not reliable for the highly blurred images because of difficulty in edge detetion. On the other hand, Frequency-based approach is based on the fact that image blur appears in the attenuation of high frequency components. HP (High-Pass) vs. BP (Band-Pass) spectral contents ratio is used in convenient as a sharpness index [12].

While, Hybrid approach C) is a more advanced method that combines the advantages of A) and B), but has the disadvantage of high computational cost.

In contrast, a simple way to measure sharpness with the gradient of the Fourier spectrum intensity that attenuates with the inverse of the frequency was also proposed [13].

An ideal method for image sharpness assessment may be any no-reference (NR) model. Recently, Z. Zhang et al., [14] proposed NR algorithm SDSM (Scale and Direction-based Sharpness Measure) constructing multiple LMM (Local-Mean Magnitude Map) based on a multiscale DCT decomposition. They evaluated the performance of SDSM statistically by comparing with typical methods using public image database and obtained the better scores than others. Though, the method combines the predefined models to induce SDSM. Hence it needs very cumbersome procedure for setting the complicated multiple parameters and lacks practicality.

Measuring Slope of Image Spectral Distribution

Since the high-frequency components in images attenuate with blur, a simple way for image sharpness assessment is to measure the attenuation of the spectral distribution.

The magnitude of image spectrum $M(\omega)$ is known to fall exponentially with reciprocal of frequency ω like as

$$M(\omega) \propto \omega^{-\alpha} \tag{13}$$

Taking the *log*arithm of $M(\omega)$

$$log\{M(\omega)\} \propto -\alpha log(\omega) \tag{14}$$

Now we can get a single sharpness index α from the line slope. It's said that the smaller the index α, the sharper the image and blurred if $\alpha > 1$.

Applying *Fourier DCT transform* $\mathcal{F}$ to the sharpened image, the 2D spectral distribution is obtained as

$$\mathcal{I}_{sharp}(\omega_x, \omega_y) = \mathcal{F}[I_{sharp}(x,y)] \tag{15}$$

For simplicity, the 2D distribution is converted to 1D by

$$\mathcal{I}_{sharp}(\omega_x, \omega_y) \rightarrow \mathcal{I}_{sharp}(\omega) \ for\ \omega = \sqrt{{\omega_x}^2 + {\omega_y}^2} \tag{16}$$

The $log\{\mathcal{I}_{sharp}(\omega)\}$ is fitted by a straight line with slope α by

$$log\{\mathcal{I}_{sharp}(\omega)\} \cong K - \alpha\omega,\ K = const \tag{17}$$

Figure 9 shows an estimated example of slope α for "*Taj Mahal*" close up in *Figure* 8 (b). The magnitude distribution of the log-transformed spectrum fluctuates greatly. Sine the fitted straight lines look unstable, α values may not be reliable.

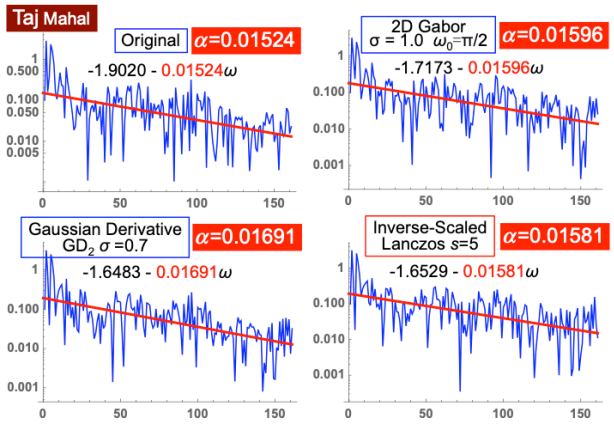

Figure 9. Estimated slope of log spectral magnitude for "Taj Mahal"

A New LMH Mapping Method for Image Spectra

In this paper, the Fourier DCT distribution is divided into *L* (*Low*), *M* (*Middle*), and *H* (*High*) frequency domains, and the integrated spectral intensity in each domain is mapped to 2-D multi-band regions for the image sharpness evaluation.

As shown in the domain map of *Figure 10* (a), the integrated spectral power Ψ in each domain is estimated by

$$\Psi(a,b,c,d) = \int_c^d \int_a^b \mathfrak{I}_{sharp}(\omega_x, \omega_y)\, d\omega_x\, d\omega_y \qquad (18)$$

The choice of integration range (*a, b, c, d*) designates Ψ in the 9 domains of (*LL, ML, HL, LM, MM, HM, LH, MH, HH*) like as

$\Psi(1, L_x, 1, L_y) = LL$; $\Psi(L_x, M_x, 1, L_y) = ML$; $\Psi(M_x, L_x, 1, L_y) = HL$; $\Psi(1, Lx, L_y, M_y) = LM$; $\Psi(L_x, M_x, L_y, M_y) = MM$; $\Psi(M_x, H_x, L_y, M_y) = HM$; $\Psi(1, Lx, M_y, H_y) = LH$; $\Psi(L_x, M_x, M_y, H_y) = MH$; $\Psi(M_x, H_x, M_y, H_y) = HH$.

Figure 10 (b) and (c) compare the sharpness factors estimated by the proposed spectral power Ψ for the sharpened images. The image sharpness is mainly reflected in the spectral power Ψ of *HH* domain. For image "*Thread*", it is shown that Gaussian Derivative $\boldsymbol{GD_2}$ is first and the proposed $\boldsymbol{LR_{Sharp}}$ is second. On the other hand, for image "*Taj Mahal*", $\boldsymbol{LR_{Sharp}}$ ranked first and ***Gabor*** ranked second. These results are generally consistent with the subjective feel, and have the advantage of quantitative evaluation against the ambiguity in the above-mentioned slope α of log spectral magnitude.

Figure 11 shows another evaluation result for image "*Genova*" taken by author's compact low-end digital camera.

The sharpened images are compared in the close up of *Figure 11*(a) . Looking carefully, the sharpening effects appear on the dial of clock tower. In this sample, ***Gabor*** is clearly inferior, proposed $\boldsymbol{LR_{Sharp}}$ looks to slightly out form to $\boldsymbol{GD_2}$ but appears to be nearly equal. The slope index α of log spectral magnitude also reflects that ***Gabor*** is the worst, and $\boldsymbol{LR_{Sharp}}$ is much the same as $\boldsymbol{GD_2}$. The proposed method also supports these results with the LHM values, but it can be said that the validity of the clear numerical evaluation could be verified.

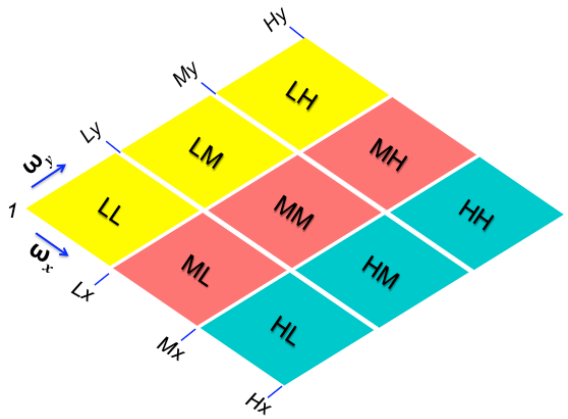

(a) LMH Fourier spectral domain map to measure sharpness factor

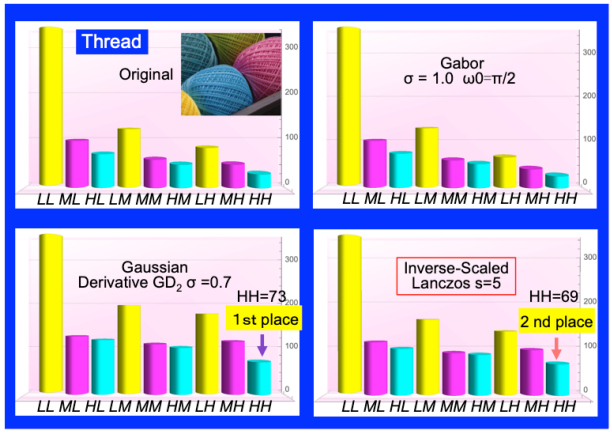

(b) *Comparisons in LMH magnitude for sharpened "Tread" image*

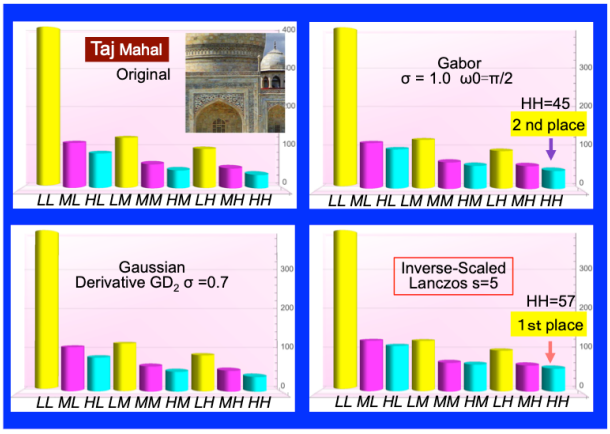

(c) *Comparisons in LMH magnitude for sharpened "Taj Mahal" image*

Figure 10. Sharpness evaluated by LMH Fourier spectral magnitude

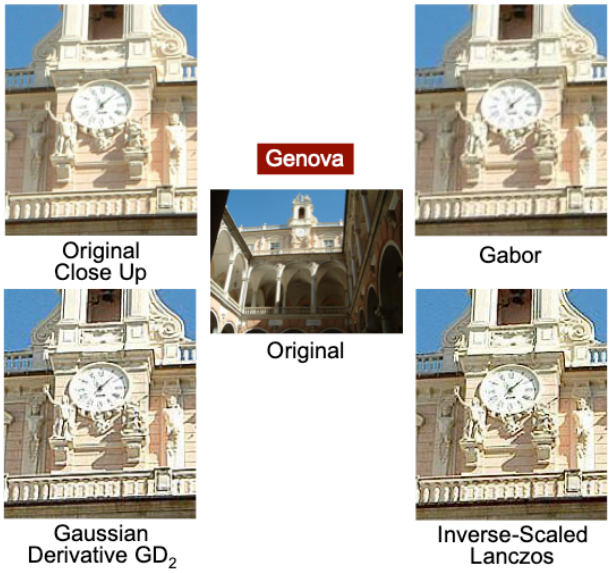

(a) ***Comparisons in the sharpened dial of clock tower for "Genova"***

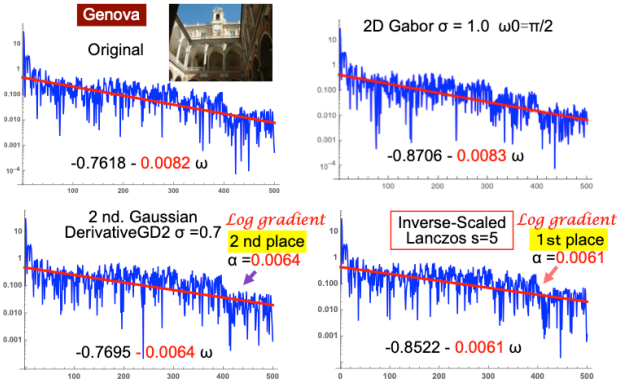

(b) ***Estimated slope α of log spectral magnitude***

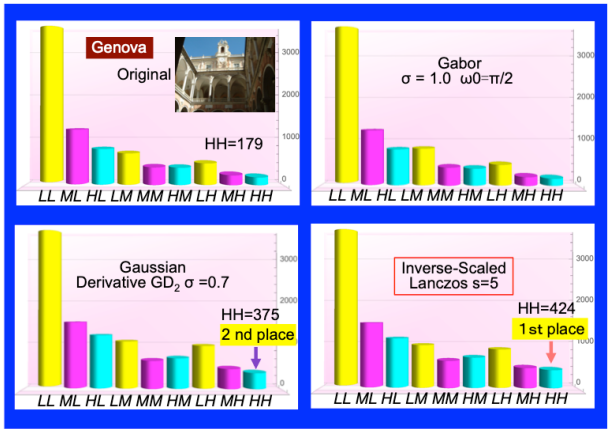

(c) ***Comparisons in LMH magnitude for sharpened "Genova" image***

Figure 11. Sharpness evaluation results for commercial camera image

Conclusions

Gabor and ***Gaussian*** second derivative ***GD₂*** functions are known as typical mathematical models of retinal receptive field.

Firstly, this paper re-examined their local compactness in space and in spatial frequency. ***GD₂*** is used for image sharpening, whereas ***Gabor*** is rarely used for sharpening. Rather, it is used for pattern recognition such as direction detection in vision research. Though, since the profile of ***Gabor*** function can be approximated to ***GD₂*** by adjusting the parameters, this article examined its effectiveness as an image sharpening filter.

Secondly, the author found that simply reversing the scale s of Lanczos Resampling function ***LR*** makes a sharp sharpening filter LR_{Sharp}. Because ***LR*** function is used to interpolate sample points, it's effective for smoothing rather than sharpening. Though, this paradoxical use led to an unexpectedly effective.

Secondly, the author found that simply reversing the scale s of Lanczos Resampling function ***LR*** makes a sharp sharpening filter LR_{Sharp}. Because ***LR*** function is used to interpolate sample points, it's effective for smoothing rather than sharpening. However, this paradoxical use led to an unexpectedly effective sharpening, especially in enhancing such a delicate wall pattern as Taj Mahal Temple.

The automatic setting of filter size and parameters adapted to the image contents is left behind as a future work.

References

[1] D. H. Hubel and T. N. Wiesel, "Receptive fields, binocular interaction and functional architecture in the cat's visual cortex", J. Physiol., Lond, 160, 106 (1962)

[2] D. G. Stork and H. R. Wilson, "Do Gabor functions provide appropriate descriptions of visual cortical receptive fields?", J. Opt. Soc. Amer., 7(8), 1362 (1990)

[3] J. Yang, "Do Gabor functions provide appropriate descriptions of visual cortical receptive fields? : comment", J. Opt. Soc. Amer., 9, 2, 334 (1992)

[4] S. A. Klein and B. Beutter, "Minimizing and maximizing the joint space-spatial frequency uncertainty of Gabor-like functions: comment", J. Opt. Soc. Amer., 9, 2, 337 (1992)

[5] D. Gabor, "Theory of communication", J. Inst. Elec. Eng., 93, 429 (1946)

[6] D. Marr and E. Hildreth, "Theory of edge detection", Proc. R. Soc. London, B207, 187 (1983)

[7] R. A. Young, Oh, say, can you see? The physiology of vision, SPIE, 1453, pg. 92. (1991)

[8] J. Daugman, "Two-dimensional analysis of cortical receptive field profiles", Vision Res., 20, 846 (1980)

[9] C. E. Duchon, "Lanczos Filtering in One and Two Dimensions", J. Applied Meteorology., 18(8), 1016 (1979)

[10] H. Kotera and Hui Wang, "Multiscale image sharpening adaptive to edge profile", J. Elect. Imaging., 14(1), 1 (2005)

[11] N. F Zhang et al., A Statistical Measure for the Sharpness of the SEM Images, Proc. SPIE, 3050, pg. 375. (1997)

[12] D. Shaked and I. Tastl, Sharpness measure: towards automatic image enhancement, Proc. IEEE ICIP, pg. 11. (2005)

[13] C. T. Vu and D. M. Chandler, A Spectral and Spatial Sharpness Measure, Proc IEEE MMEDIA, pg. 37. (2009)

[14] Z. Zhang et al., No-Reference Image Sharpness Assessment Using Scale and Directional Models, Proc. IEEE ICME, (2018)

Author Biography

Hiroaki Kotera *joined Panasonic in 1963. He received PhD from Univ. of Tokyo. After worked at Matsushita Res. Inst. Tokyo during 1973-1996, he was a professor at Chiba University. He retired in 2006 and is collaborating with Chiba University. He received 1993 IS&T honorable mention, 1995 SID Gutenberg prize, 2005 IEEE Chester Sall award, 2007 IS&T Raymond. C. Bowman award, 2009 SPSTJ and 2012 IIEEJ best paper awards. He is a Fellow of IS&T and IIEEJ.*